Structural Engineering and Mechanics, Vol. 25, No. 1 (2007) 91-106
DOI: http://dx.doi.org/10.12989/sem.2007.25.1.091

(4+*n*)-noded Moving Least Square(MLS)-based finite elements for mesh gradation

Jae Hyuk Lim† and Seyoung Im‡

Department of Mechanical Engineering, Korea Advanced Institute of Science and Technology (KAIST), Science Town, Daejeon 305-701, Republic of Korea

(Received May 23, 2006, Accepted August 16, 2006)

Abstract. A new class of finite elements is described for dealing with mesh gradation. The approach employs the moving least square (MLS) scheme to devise a class of elements with an arbitrary number of nodal points on the parental domain. This approach generally leads to elements with rational shape functions, which significantly extends the function space of the conventional finite element method. With a special choice of the nodal points and the base functions, the method results in useful elements with polynomial shape functions for which the C^1 continuity breaks down across the boundaries between the subdomains comprising one element. Among those, $(4 + n)$-noded MLS based finite elements possess the generality to be connected with an arbitrary number of linear elements at a side of a given element. It enables us to connect one finite element with a few finite elements without complex remeshing. The effectiveness of the new elements is demonstrated via appropriate numerical examples.

Keywords: MLS-based finite elements; moving least square approximation; mesh gradation; stress concentration.

1. Introduction

When steep stress gradients or singularities exist due to the configuration of geometry or local concentrated loads, finite element mesh should be refined locally. Such mesh refinement often leads to highly distorted elements or meshes consisting of excessive number of nodes to maintain the quality of mesh. In addition, one of the major difficulties is to maintain the element connectivity, which is required for compatible meshes. It is far from being trivial to meet the connectivity of elements for complex domains, such as, nonmatching meshes, contact problems and mesh gradation. For example, when a group of mesh designers construct a large scale finite element model like an airplane, each of the mesh designers models his own part, and later all parts are joined together to construct the entire structure. In such a circumstance, it requires a tremendous amount of labor to construct meshes meeting the element connectivity along the interface of two neighboring parts.

To resolve this, Gupta (1978) developed a two dimensional transition element to join one bilinear element to two bilinear elements at the edge of elements for mesh gradation. Choi and Lee (1993, 1996) succeeded in developing three dimensional transition solid elements and Choi and Park

† E-mail: ljh77@kaist.ac.kr
‡ Professor, Corresponding author, E-mail: sim@kaist.ac.kr

(1989, 1997) also developed transition plate elements, and utilized them for adaptive mesh refinement. These approaches seem to be quite reasonable for fulfilling the compatibility without any ambiguity but it does not possess a generality to handle elements more than two at the side of element. To resolve this issue, various techniques, such as two or three layer approaches with Lagrange multipliers or penalty function parameters (Farhat and Roux 1991, Aminpour *et al.* 1995, 1998, Quiroz and Beckers 1995, Pantano and Averill 2002, Park *et al.* 2002) and Interface Element Method (Kim 2002) are proposed. In the two or three layer approaches, constraints are added to meet compatibility at the interfaces. In IEM (Interface Element Method), nonmatching finite element zones are treated as meshfree domain, and nodes are appropriately added to fulfill the mesh compatibility. However, the above-mentioned schemes are partially successful in dealing with dissimilar meshes in that their practical applications for three dimensional problems are not available.

For the simplification of IEM, Cho *et al.* (2005) suggested Improved Interface Element Method by constructing a new class of master element with variable number of nodes via MLS approximation. With this idea, MLS-based variable node elements for handling a number of nonmatching meshes (Cho and Im 2006) and propagating cracks (Cho and Im 2006) were also proposed. This element-based approach is so simple that we can implement the present algorithm into any existing finite element codes in a straightforward manner. Despite this outstanding feature, rational type shape functions from MLS-approximations are still an impediment to application for various problems due to the difficulty in numerical integration. Even a high order Gaussian integration such as 6×6 involves an error as large as one percent. Recently, Lim *et al.* (2006) developed modified MLS variable node elements the so-called MLS-based finite elements in the two and three-dimensional framework such as $(4+n)$-noded elements, $(9+2n)$-noded elements, $(8+2m+2n+mn)$-noded elements and so forth. Although their shape functions are generated from MLS-approximation, they reduce to the polynomial type by making a careful choice of the bases and by controlling the domain of influence of each node. Applications for various nonmatching mesh problems turn out to be successful even with lower order Gaussian integration, such as 2×2 per each subdomain for bilinear polynomial bases. This is in a striking contrast with the MLS-variable node elements reported in references (Cho *et al.* 2005, Cho and Im 2006). Particularly, the new MLS-based finite elements are tractable to $\overline{B}$-approach for treating the incompressibility constraints occurring in elastic-plastic deformations.

In this paper, we focus on exhibiting another applications of $(4+n)$-noded elements for mesh gradation, which did not discussed in the previous works. $(4+n)$-noded MLS-based finite elements possess the generality to handle an arbitrary number of bilinear elements on its side and provide the convenience for modeling of zone of high stress concentration, allowing outstanding mesh gradation between fine mesh and coarse mesh.

The outline of the paper is as follows. We provide a brief review of the MLS method, and this is followed by the formulation of the MLS-based finite elements. In Section 3, we show that a special choice in the present scheme leads to useful $(4+n)$-noded finite elements with polynomial shape functions. Next we provide some numerical examples to demonstrate the effectiveness and accuracy of this methodology. All numerical examples show that the MLS-based elements are extremely useful in capturing high stress concentration like a hole or a corner using mesh gradation. Finally, we wrap up the paper with some concluding remarks.

2. Moving Least Square (MLS) method and MLS-based finite elements

In this section, we briefly describe the MLS method (Lancaster 1981), and then explain how to construct the shape functions of MLS-based finite elements. Let $\mathbf{u}(\boldsymbol{\xi})$ be a two-dimensional vector field, and $u_\alpha(\alpha = 1, 2)$ its two components, interchangeably denoted by (u, v). The independent variable $\boldsymbol{\xi}$ indicates the master coordinate (ξ_1, ξ_2), interchangeably indicated by (ξ, η) whenever it is convenient. Suppose we want a MLS approximation $\mathbf{u}^h(\boldsymbol{\xi}, \bar{\boldsymbol{\xi}})$ for $\mathbf{u}(\boldsymbol{\xi})$ in terms of NB base-polynomials, where $\bar{\boldsymbol{\xi}}$ denotes the center of a circle within which this approximation is taken. Then $\mathbf{u}^h(\boldsymbol{\xi}, \bar{\boldsymbol{\xi}})$ is given as

$$\mathbf{u}^h(\boldsymbol{\xi}, \bar{\boldsymbol{\xi}}) = \mathbf{a}^T(\bar{\boldsymbol{\xi}})\mathbf{p}(\boldsymbol{\xi} - \bar{\boldsymbol{\xi}}) \tag{1}$$

where $\mathbf{a}^T(\bar{\boldsymbol{\xi}})$ is the $2 \times \mathrm{NB}$ matrix of the unknown coefficients depending on $\bar{\boldsymbol{\xi}}$, and $\mathbf{p}(\boldsymbol{\xi} - \bar{\boldsymbol{\xi}})$ is a $\mathrm{NB} \times 1$ column matrix of the shifted polynomial basis i.e.,

$$\mathbf{p}^T(\boldsymbol{\xi} - \bar{\boldsymbol{\xi}}) = [1, \xi - \bar{\xi}, \eta - \bar{\eta}, (\xi - \bar{\xi})(\eta - \bar{\eta}), (\xi - \bar{\xi})^2, (\eta - \bar{\eta})^2, \ldots] \tag{2}$$

The shifted polynomial basis enables us to remove the numerical stability problem from the nonshifted polynomial basis (Jin *et al.* 2001). The functional to be minimized in the least square sense is given as

$$J(\mathbf{a}^T(\bar{\boldsymbol{\xi}})) = \sum_{I=1}^{NP} [\mathbf{a}^T(\bar{\boldsymbol{\xi}})\mathbf{p}(\boldsymbol{\xi}_I - \bar{\boldsymbol{\xi}}) - \mathbf{u}_I]^T [\mathbf{a}^T(\bar{\boldsymbol{\xi}})\mathbf{p}(\boldsymbol{\xi}_I - \bar{\boldsymbol{\xi}}) - \mathbf{u}_I] w_I(\boldsymbol{\xi}_I - \bar{\boldsymbol{\xi}}) \tag{3}$$

where $I = 1$~NP indicates a particle or a nodal point, and w_I and $\mathbf{u}_I$ are the weight function and the nodal value of $\mathbf{u}(\boldsymbol{\xi})$ associated with the particle "I", respectively. By minimizing this functional, we obtain the following equation for $\mathbf{a}(\bar{\boldsymbol{\xi}})$:

$$\frac{\partial J}{\partial \mathbf{a}} = \mathbf{M}(\bar{\boldsymbol{\xi}})\mathbf{a}(\bar{\boldsymbol{\xi}}) - \mathbf{B}\mathbf{U} = \mathbf{0} \quad \text{with} \quad \mathbf{M} = \mathbf{P}\mathbf{W}\mathbf{P}^T \quad \text{and} \quad \mathbf{B} = \mathbf{P}\mathbf{W} \tag{4}$$

where $\mathbf{P} = \mathbf{P}(\boldsymbol{\xi}_I - \bar{\boldsymbol{\xi}})$, $\mathbf{W} = \mathbf{W}(\boldsymbol{\xi}_I - \bar{\boldsymbol{\xi}})$, and $\mathbf{U}$ are given as

$$\mathbf{P} = \begin{bmatrix} 1 & 1 & 1 & \cdots & 1 \\ (\xi_1 - \bar{\xi}) & (\xi_2 - \bar{\xi}) & (\xi_3 - \bar{\xi}) & \cdots & (\xi_{NP} - \bar{\xi}) \\ (\eta_1 - \bar{\eta}) & (\eta_2 - \bar{\eta}) & (\eta_3 - \bar{\eta}) & \cdots & (\eta_{NP} - \bar{\eta}) \\ (\xi_1 - \bar{\xi})(\eta_1 - \bar{\eta}) & (\xi_2 - \bar{\xi})(\eta_2 - \bar{\eta}) & (\xi_3 - \bar{\xi})(\eta_3 - \bar{\eta}) & \cdots & (\xi_{NP} - \bar{\xi})(\eta_{NP} - \bar{\eta}) \\ (\xi_1 - \bar{\xi})^2 & (\xi_2 - \bar{\xi})^2 & (\xi_3 - \bar{\xi})^2 & \cdots & (\xi_{NP} - \bar{\xi})^2 \\ (\eta_1 - \bar{\eta})^2 & (\eta_2 - \bar{\eta})^2 & (\eta_3 - \bar{\eta})^2 & \cdots & (\eta_{NP} - \bar{\eta})^2 \\ \cdots & \cdots & \cdots & \cdots & \cdots \\ \cdots & \cdots & \cdots & \cdots & \cdots \end{bmatrix}_{NB \times NP}$$

$$\mathbf{W} = \begin{bmatrix} w_1(\xi_1 - \bar{\xi}) & 0 & 0 & 0 & \dots & 0 \\ 0 & w_2(\xi_2 - \bar{\xi}) & 0 & 0 & \dots & 0 \\ 0 & 0 & w_3(\xi_3 - \bar{\xi}) & 0 & \dots & 0 \\ 0 & 0 & 0 & w_4(\xi_4 - \bar{\xi}) & \dots & 0 \\ \dots & \dots & \dots & \dots & \dots & \dots \\ \dots & \dots & \dots & \dots & \dots & \dots \\ 0 & 0 & 0 & 0 & \dots & w_{NP}(\xi_{NP} - \bar{\xi}) \end{bmatrix}_{NP \times NP}$$

$$\mathbf{U}^T = \begin{bmatrix} u_1 & u_2 & u_3 & \dots & u_{NP} \\ v_1 & v_2 & v_3 & \dots & v_{NP} \end{bmatrix}_{2 \times NP}$$

Plugging $\mathbf{a}(\bar{\xi})$ from Eq. (4) into (1), we have

$$\mathbf{u}^h(\xi, \bar{\xi}) = \mathbf{U}^T\mathbf{B}^T(\bar{\xi})\mathbf{M}^{-1}(\bar{\xi})\mathbf{p}(\xi - \bar{\xi}) = \sum_{I=1}^{NP} \phi_I(\xi, \bar{\xi})\mathbf{u}_I \tag{5}$$

Taking the moving process $\lim_{\bar{\xi} \to \xi} \mathbf{u}^h(\xi, \bar{\xi}) = \mathbf{u}^h(\xi)$ in Eq. (5), we reach the following equation

$$\lim_{\bar{\xi} \to \xi} \mathbf{P}^T(\xi - \bar{\xi}) = \mathbf{P}^T(0) = [1, 0, 0, 0, 0, 0, 0, \dots]$$

$$\mathbf{u}^h(\xi) = \mathbf{U}^T\mathbf{B}^T(\xi)\mathbf{M}^{-1}(\xi)\mathbf{p}(0) = \sum_{I=1}^{NP} \phi_I(\xi)\mathbf{u}_I \tag{6}$$

where $\mathbf{u}_I$ is the nodal vector of the node "I", which is the I-th column vector of $\mathbf{U}^T$, and the shape function $\phi_I(\xi)$ is given as

$$\phi_I(\xi) = \sum_{L=1}^{NB} \sum_{J=1}^{NB} B_{LI}(\xi)M_{LJ}^{-1}(\xi)p_J(0) = \sum_{L=1}^{NB} B_{LI}(\xi)b_L(\xi) \tag{7}$$

where $b_L(\xi) = \sum_{J=1}^{NB} M_{LJ}^{-1}(\xi)p_J(0)$

With the complete linear polynomial being included in $\mathbf{p}(\xi - \bar{\xi})$, the MLS-based shape function (7) satisfies the following conditions due to its polynomial reproducing property (Liu *et al.* 1995).

$$\text{Partition of unity:} \quad \sum_{I=1}^{NP} \phi_I(\xi) = 1 \tag{8}$$

$$\text{Linear completeness:} \quad \sum_{I=1}^{NP} \phi_I(\xi)\xi_I = \xi \tag{9}$$

Despite the satisfaction of these two conditions, we are not yet fully assured that $\phi_I(\xi)$ may be utilized for the shape functions of finite element method. To discuss this point further, we consider an element shape function given by Eq. (7) for a square parental domain. From this parental domain

(ξ_1, ξ_2) to the physical domain (x_1, x_2), we choose an isoparametric mapping. Then, we have

$$x_\alpha(\boldsymbol{\xi}) \equiv x_\alpha(\xi_1, \xi_2) = \sum_I \phi_I(\boldsymbol{\xi}) x_{\alpha I} \tag{10a}$$

$$u_k(\boldsymbol{\xi}) \equiv u_k(\xi_1, \xi_2) = \sum_I \phi_I(\boldsymbol{\xi}) u_{kI} \tag{10b}$$

where $\alpha = 1, 2$ and $-1 \le \xi_\alpha \le 1$.

We now discuss the suitability of the above $\phi_I(\boldsymbol{\xi})$ for a shape function of finite element methods. Firstly, the existence of $\phi_I(\boldsymbol{\xi})$ may be addressed from Eq. (7), which shows that the moment matrix $\mathbf{M}(\boldsymbol{\xi})$ should be invertible for the existence of $\phi_I(\boldsymbol{\xi})$. A slightly enforced form of this condition appears in the form of the so-called "theorem for admissible particle distributions" (Han and Meng 2001), which states the following requirement for the case of one-dimensional domain $-1 \le \xi \le 1$: every internal point of the domain should be covered at least by distinct NB particles or nodal points, which means that within the domain of influence of an arbitrary internal point, distinct active NB nodes should exist. This theorem was extended, by Han and Meng (2001), to the case of the multi-dimensional domain wherein only linear polynomials are employed for the bases. The key element is that the matrices **P** and $\mathbf{W}(\boldsymbol{\xi})$ or the distribution of the nodal points and the weight function matrix should be chosen such that the moment matrix $\mathbf{M}(\boldsymbol{\xi})$ may be invertible and well-conditioned. In this context, to assure the validity of a given particle distribution and weight function matrix for multi-dimensional domains with the higher order polynomials for the bases, we require that the rank of the matrix **P** should be equal to NB and that the rank of $\mathbf{W}(\boldsymbol{\xi})$ should not be smaller than NB in the interior of the domain. In addition, the norm of the inverse moment matrix should be bounded properly. Hereafter we denote the rank of $\mathbf{W}(\boldsymbol{\xi})$ by Rank (**W**) for further discussion.

It is straightforward to find from Eqs. (8) and (10a) that the linear completeness condition is satisfied on the physical domain. Presuming that the C^1 continuity is satisfied in the element interior, the remaining requirement for finite element shape function comes from the compatibility and the aspect of imposing displacement boundary conditions. In this context, we examine the following two conditions:

Condition 1: $\phi_I(\boldsymbol{\xi})$ should disappear along all element edges not meeting with its node "I"

Condition 2: $\phi_I(\boldsymbol{\xi})$ should be zero at all nodes other than node "I", i.e., Kronecker delta condition $\phi_I(\boldsymbol{\xi}_J) = \delta_{IJ}$

To discuss these two conditions in detail, we separately consider the two cases: one wherein Rank(**W**) is greater than NB, the number of the base polynomials, and the other wherein Rank(**W**) is equal to NB.

2.1 MLS-based elements with Rank(W) greater than NB

If Rank(**W**) is greater than NB, the approximation (10b) is in the nature of MLS approximation on the element domain. To explain the two conditions above, we take a simple case shown in Fig. 1. This depicts a 5-noded MLS-based element, and the complete linear polynomial $[1, \xi, \eta]^T$ is chosen for the basis $\mathbf{p}(\boldsymbol{\xi})$. The element was utilized by Cho *et al.* (2005) to treat nonmatching

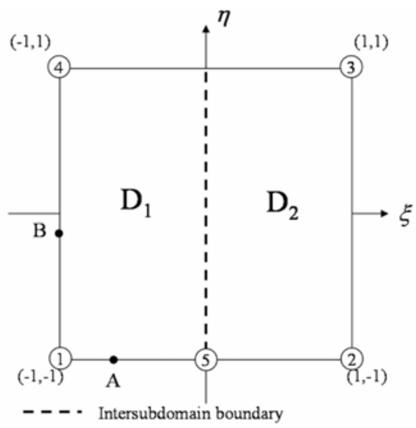

Fig. 1 A master element of a 5-noded MLS-based element

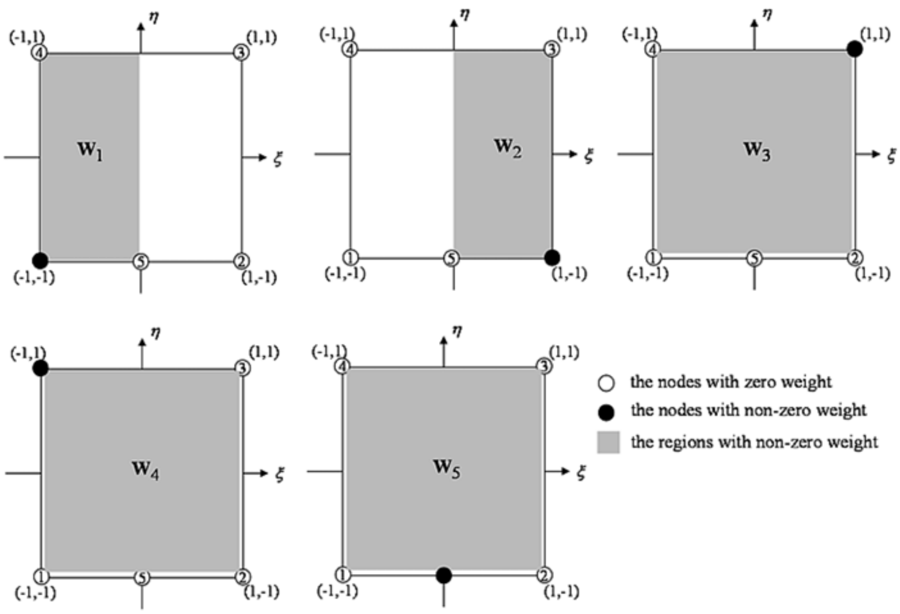

Fig. 2 Domains of influence of a 5-noded MLS-based element

meshes of 4-noded plane elements. The entire element domain consists of two subdomains, D_1 and D_2, as shown in Fig. 1. We let each support of the weight functions w_3, w_4 and w_5 cover the whole element domain, while the support of w_1 is restricted to D_1 and the support of w_2 to D_2. Then Rank($\mathbf{W}$) is equal to 4 on each of the two subdomains D_1 and D_2, and this is greater than NB, which is 3.

We presume that a bell type function, which vanishes smoothly on its support boundary, is employed for every weight function. The behavior of each weight function is plotted in Fig. 2. Note that each weight function is zero at all nodes except for its own node so that every point on the element boundary is covered by the two weight functions of the two nodes between which the point lies. For example, point "A" ($\xi = -0.6$ and $\eta = -1$) is covered by w_1 and w_5, while point "B" ($\xi = -1$ and $\eta = -0.1$) is covered by w_1 and w_4. In such circumstances, each shape function given by Eq. (7) vanishes smoothly on the part of the element boundary where the corresponding weight function smoothly goes to zero. Thus, shape function $\phi_I(\boldsymbol{\xi})$ disappears along all element edges not meeting with node "I", and Condition 1 is fulfilled.

To explain Condition 2, we now examine the behavior of the shape functions when we approach a part of the element boundary from the element interior, say the boundary $-1 \le \xi \le 0$ and $\eta = -1$. For convenience, by RankB(**W**) and NBB, hereafter we denote the rank of the weight function matrix $\mathbf{W}(\boldsymbol{\xi})$ and the number of the active base polynomials on the element boundary, respectively. As the element boundary $\eta = -1$ is approached, the base polynomials reduce to (1, ξ), and, therefore, we obtain NBB=2. As far as every point on the boundary $-1 \le \xi \le 0$ and $\eta = -1$ is covered by w_1 and w_5, we have the condition RankB(**W**)=NBB=2, and then the shape function $\phi_I(\xi, \eta)$ ($I = 1$ and 5) reduces to a point interpolation, given as a linear function of ξ in the limit on this boundary. The same argument applies to the boundary $0 \le \xi \le 1$ and $\eta = -1$, and the remaining element boundary. As one approaches the boundary from the interior, every limit point on the boundary lies between two nodes, and in the limit the unknown variable u_α at this point is linearly interpolated by the values of these two nodes (see Cho *et al.* (2005) for proof via explicit calculation). From this and Condition 1, we see that each shape function meets the Kronecker delta condition. However, the expression of $\phi_I(\xi, \eta)$ in the element interior is a complex rational function, which becomes a linear function in the limit on the element boundary. This element was successfully employed for treating nonmatching meshes composed of 4-noded bilinear elements, but one drawback was that higher order Gaussian integration, i.e., 6×6 integration on each of D_1 and D_2, was used to pass the patch test. In the next subsection we will suggest an improved element, which will help to surmount this shortcoming.

2.2 MLS-based elements with Rank(W) equal to NB

Although the MLS-based shape function $\phi_I(\boldsymbol{\xi})$ discussed in the previous subsection, though it satisfies "Conditions 1 and 2" on the boundary nodes, it is not the conventional polynomial interpolation, as it is in the nature of the moving least square approximation in the interior of the domain. In the element interior, the shape function $\phi_I(\boldsymbol{\xi})$ belongs to a class of rational function. The examples of this type of variable-node elements was introduced in Cho *et al.* (2005) and Cho and Im (2006) together with some applications for nonmatching meshes and crack propagation. However, the shortcoming of these elements is that they require an integration order as high as 6×6 Gaussian integration since $\phi_I(\boldsymbol{\xi})$ are of the rational function type.

In this subsection, we explore the suitability of the case Rank(**W**)=NB for finite element shape function. If Rank(**W**)=NB pointwise and a proper choice of the polynomial bases is made, the shape function $\phi_I(\boldsymbol{\xi})$ becomes a point interpolation over the entire domain and it reduces to a polynomial that has nothing to do with the choice of the form of the weight function. This observation is straightforward from the first equality of Eq. (6). However, this does not imply that the resulting element for Rank(**W**)=NB is simply nothing but the existing conventional finite elements. Even in the case of the equality, the present approach results in a new class of finite elements, which we can endow with variable number of nodes by properly choosing the support of the weight function of each element node. The restriction of the support of each weight function only to some part of the element domain, not taking the entire domain for each of the supports, means that we let the element be comprised of subdomains, each of which is covered by a different set of weight functions.

This also implies the relaxation of the C^1 continuity along the intersubdomain boundaries. Note that C^1 continuity is not required in the pointwise sense on the element domain as long as the discontinuity of derivatives is taken into account in the numerical integration. Note that the continuity of traction or the equilibrium across the surface wherein this breaks down is imposed in the weak form sense in finite element methods.

Consider the two-dimensional parental domain again in Fig. 1. We maintain the same nodes 1 through 5 and the same subdomains D_1 and D_2 as in Fig. 1, but for the basis we choose the polynomials up to the bilinear term

$$\mathbf{p} = [1, \xi, \eta, \xi\eta]^T \tag{11}$$

on each of the two subdomains. Then we have Rank (W)=NB=4 on each of the subdomains, and the expression (7) for the shape functions now reduces to a typical point interpolation:

$$\boldsymbol{\varphi}(\boldsymbol{\xi}) = \mathbf{P}^{-1}(\boldsymbol{\xi}_I - \bar{\boldsymbol{\xi}})\mathbf{p}(\mathbf{0}) \tag{12}$$

where

$$\boldsymbol{\varphi}(\boldsymbol{\xi}) = \begin{cases} [\phi_1(\boldsymbol{\xi}), \phi_3(\boldsymbol{\xi}), \phi_4(\boldsymbol{\xi}), \phi_5(\boldsymbol{\xi})]^T \text{ and } \phi_2(\boldsymbol{\xi}) = 0.0 \text{ on } D_1 \\ [\phi_2(\boldsymbol{\xi}), \phi_3(\boldsymbol{\xi}), \phi_4(\boldsymbol{\xi}), \phi_5(\boldsymbol{\xi})]^T \text{ and } \phi_1(\boldsymbol{\xi}) = 0.0 \text{ on } D_2 \end{cases}$$

and the matrix $\mathbf{P}$ is constructed separately on each of the subdomains, D_1 and D_2, consistent with the definition of $\boldsymbol{\varphi}(\boldsymbol{\xi})$ above. Compared with the MLS-based elements of Fig. 1 in the previous subsection, we need to take note of the following differences:

Remark 1: Condition 2 or the Kronecker delta condition is trivially satisfied in the present case because of the property of point interpolation.
Remark 2: Condition 1 may be violated, so that the interelement compatibility may not hold.
Remark 3: Discontinuity in shape function may occur across the boundary between the two subdomains, which corresponds to $\xi = 0$ in the present example.

All the above differences are linked with point interpolation, in which the smoothing role of the weight function is negated. In point interpolation, the weight function matrix $\mathbf{W}(\boldsymbol{\xi})$ may be thought of as an identity matrix on its support, but suddenly collapsing to zero matrix outside its support, so that it has the property like the step function (Liu *et al.* 2004). Despite the advantage that the Kronecker delta condition is fully satisfied, failure to meet Condition 1 and the discontinuity across the intersubdomain boundary may severely restrict the usefulness of the present class of the elements. However, we will show that some choice of the node distribution and the basis function leads to an extremely useful and efficient element.

We will now focus again on the element of Fig. 3 to examine Condition 1 and check the continuity across the intersubdomain boundary. The presence of the bilinear term, $\xi\eta$, in $\mathbf{p}$ makes it possible for $\phi_I(\boldsymbol{\xi})$ to vanish along the boundary edges not containing node $\boldsymbol{I}$ in this element, as opposed to the previous case in Fig. 2. This may be confirmed numerically, particularly if NB is a

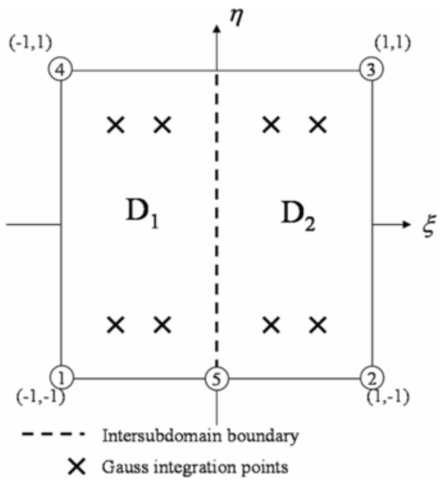

Fig. 3 Master element of the 5-noded MLS-based element and its integration points

large number. Furthermore, we can numerically verify the continuity of $\phi_I(\xi)$ across the intersubdomain boundary $\xi = 0$.

Since point interpolation results in polynomial shape functions, the use of the 2×2 Gaussian integration is sufficient on each of the two subdomains of this MLS-based element (see Fig. 3). This is a significant advantage of the present type of elements (Rank(**W**)=NB) over the previous case (Rank(**W**)>NB). It turns out that the element in Fig. 3 will pass the patch test exactly with such a simple integration. This aspect enables straightforward applications of the current type of MLS-based elements for a class of problems involving an implicit constraint, such as the plastic incompressibility. That is, the well-known $\bar{B}$ approach is applicable as easily as in the conventional finite elements.

3. (4 + *n*)-noded MLS-based elements

In this section, we illustrate $(4+n)$-noded MLS-based finite elements which can treat an arbitrary number of nodes at the element edges for mesh gradation. Every boundary segment of element composed of two neighbor nodes represents the linear interpolation. Some of elements show the polynomial type shape function integrable by simple 2×2 Gaussian integration in element interior. In Fig. 3, we already explained how to construct a 5-noded MLS-based element with bilinear interpolation function. The extension of this to a generic $(4+n)$-noded element ($n = 1, 2, 3\ldots$) is straightforward. We simply choose $\mathbf{p} = [1, \xi, \eta, \xi\eta]^T$ for the polynomial basis. Taking $n = 3$ for instance, as shown in Fig. 4, we have four subdomains, D_1, D_2, D_3, and D_4. The active nodes on each of the subdomains are as indicated in Fig. 4. One can confirm that Condition 1 is fulfilled, and that all shape functions are continuous across each of the intersubdomain boundaries $\xi = -0.5, 0.0, 0.5$. For numerical integration, simple 2×2 Gauss integration are sufficient.

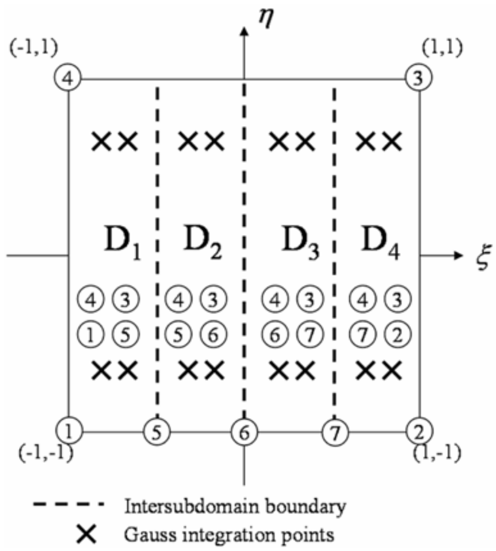

Fig. 4 A $(4+n)$-noded MLS-based element with linear interpolation on one of the boundary edges and active nodes per subdomain for $n=3$

4. Numerical examples

To demonstrate the performance of $(4+n)$-noded elements, some numerical benchmark problems are treated in this section. For checking a convergence of the elements, we conduct a series of patch test for $(4+n)$-noded elements. Second, we deal with a cantilever beam problem with mesh refinement for capturing stress gradient on the corner. As a final example, we solve an infinite plate problem including a hole with element subdivision. In these examples, we employ our in-house code, but the present elements may be easily inserted into any commercial codes, using a special tool provided, for example, UEL in the case of ABAQUS.

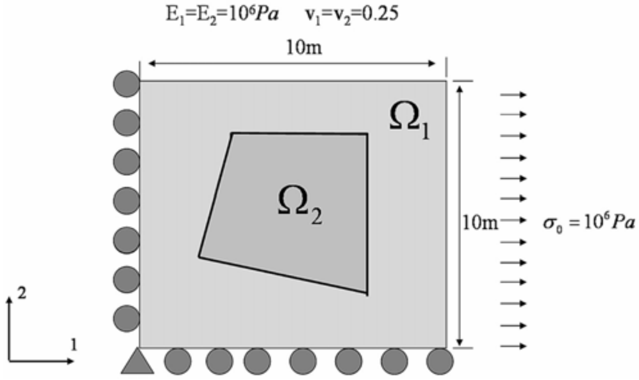

Fig. 5 Geometry and boundary conditions of the patch test for $(4+n)$-noded elements

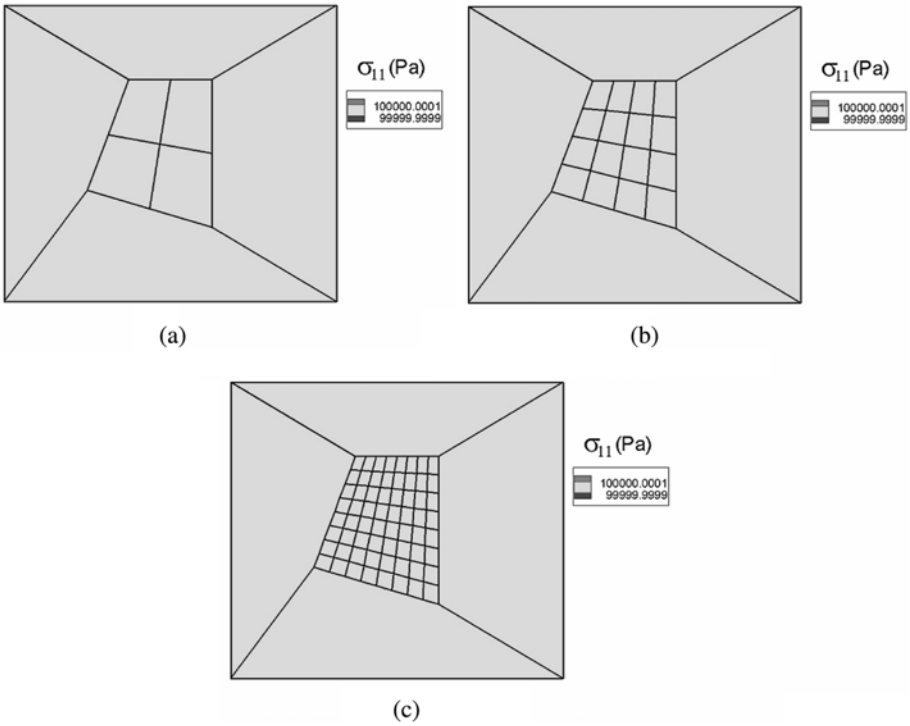

Fig. 6 The σ_{11} contour plot of patch test with a various number of elements: (a) 1st adaptation result, (b) 2nd adaptation result, (c) 3rd adaptation result

4.1 Patch test

For linear MLS-based elements, we construct a finite element mesh containing a skewed zone, as shown in Fig. 5. We model the inner region Ω_2 as 4-noded bilinear elements and the outer region Ω_1 as MLS $(4+n)$-noded elements. We impose uniform stress distribution along the right boundary of the patch and apply appropriate boundary conditions to eliminate rigid body motion, as shown in Fig. 5. Both of the material properties are $E_1 = E_2 = 10^6$ Pa and $\nu_1 = \nu_2 = 0.25$, and plane stress condition is assumed. We conduct a series of patch test for a different number of 4 noded-elements by taking subdivision of Ω_2 region. The contours of σ_{11} are plotted in Figs. 6(a)~6(c). As seen in these Figs. 6(a)~6(c), the patch test is passed clearly and no dependency on the number of elements is observed.

4.2 A cantilever beam with a tip load

As our second example, a cantilever beam is selected to investigate the performance of $(4+n)$-noded elements. The exact displacement is given as the reference (Timoshenko and Goodier 1970). where, $I = D^3/12$, $D = 2c = 10.0$ m, $L = 20.0$ m, $E_1 = E_2 = 10^6$ Pa and $\nu_1 = \nu_2 = 0.25$. The vertical traction $P(=2.5 \times 10^4\,\text{N})$ is applied at the left end of beam in Fig. 7 and plane stress condition is assumed.

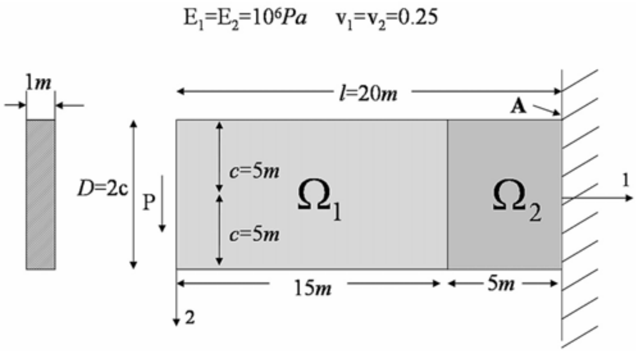

Fig. 7 Problem description of a cantilever under a tip load

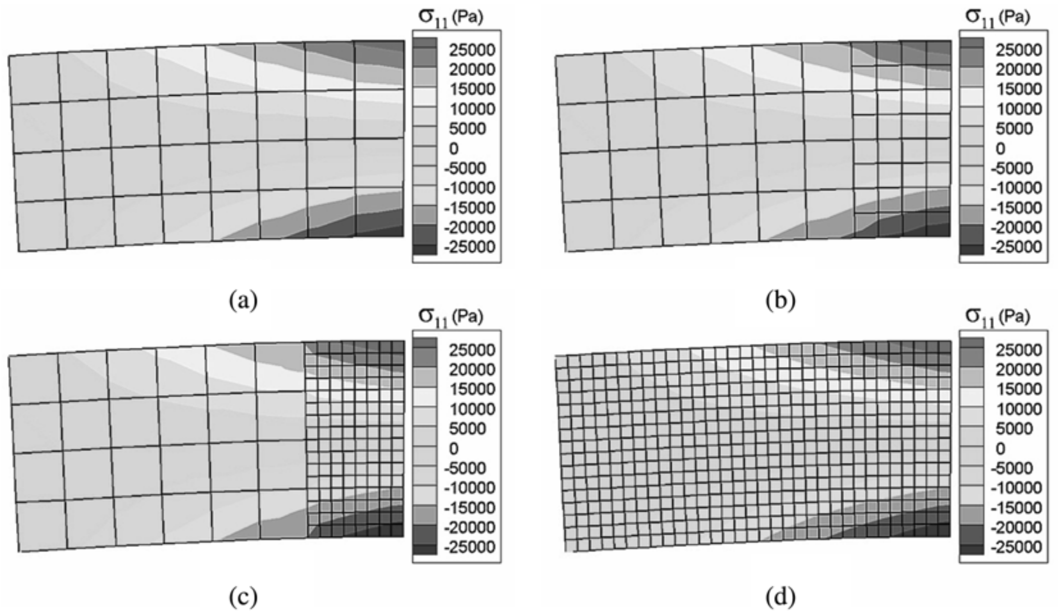

Fig. 8 The σ_{11} contour plot of a cantilever problem: (a) Initial mesh result (45 nodes), (b) 1st adaptation result (75 nodes), (c) 2nd adaptation result (183 nodes) (d) 2nd reference result (561 nodes)

$$u = -\frac{Px^2y}{2EI} - \frac{\nu Py^3}{6EI} + \frac{Py^3}{6IG} + \left(\frac{Pl^2}{2EI} - \frac{Pc^2}{2IG}\right)y$$

$$v = \frac{\nu Pxy^2}{2EI} + \frac{Px^3}{6EI} - \frac{Pl^2x}{2EI} + \frac{Pl^3}{3EI}$$

We take the sequential refinement of Ω_2 for capturing the high stress gradient on the corner of plate as seen in Figs. 8(b) and 8(c). For treating nonmatching meshes from element subdivision, we replace elements adjacent to Ω_2 in Ω_1 by $(4 + n)$-noded elements. We calculate the relative error in energy norm in Ω_2 comprised of 4-noded bilinear elements and the maximum stress value on the

Table 1 Comparison of the maximum σ_{11} stress and relative error in energy norm between reference meshes and adaptation meshes

	Maximum σ_{11} stress at Point "A" σ_{exact} = 30000 (Pa)	Relative error in energy norm at Ω_2
Coarse mesh (45 nodes)	28218.2	0.1753
Adaptation mesh 1 (75 nodes)	29282.7	8.945×10^{-2}
Reference mesh 1 (153 nodes)	29307.6	8.875×10^{-2}
Adaptation mesh 2 (183 nodes)	29705.5	4.576×10^{-2}
Reference mesh 2 (561 nodes)	29710.3	4.454×10^{-2}

corner 'A' by L_2 projection (Hinton *et al.* 1974) to compare with the results of reference meshes. To obtain the reference solutions, we make subdivision one time (reference mesh 1) and two times (reference mesh 2, Fig. 8(d)) on the original coarse matching mesh (Fig. 8(a)). As summarized in Table 1, the results of proposed scheme have an excellent agreement with the results of the reference mesh although the nodes less than the half of the nodes of the reference mesh are used to construct finite element model.

4.3 An infinite plate with a hole under tension

For the last example, we choose an infinite plate including a hole. The radius of a hole is 0.3. We only use a quarter model by imposing a proper boundary condition as depicted in Fig. 9. To capture high stress concentration, we take subdivision on Ω_2 and replace, by $(4+n)$-noded elements, these elements that are located on the inner region of Ω_1 and neighboring Ω_2. The plane is subjected to a uniform tension $\sigma_0 = 1$ in the horizontal direction. The dimensions and material properties are 1×1 square plate with a hole (see Fig. 9), and both of Young's modulus and Poisson ratio are 10^6 Pa and 0.3, respectively, and plane strain condition is assumed. To realize the infinite state in a finite body, we calculate the exact nodal forces by integrating exact stress distribution given in the reference (Timoshenko and Goodier 1970) with 12 order Gaussian integration along the boundary and impose them on the outer boundary.

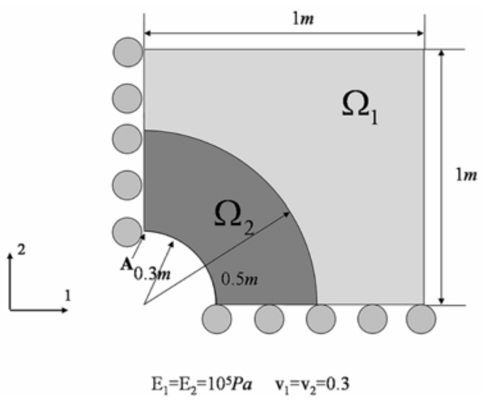

Fig. 9 Geometry and boundary conditions of an infinite plate including a hole

$$\sigma_{11}(r,\theta) = \sigma_0\left(1 - \frac{a^2}{r^2}\left(\frac{3}{2}\cos 2\theta + \cos 4\theta\right) + \frac{3}{2}\frac{a^4}{r^4}\cos 4\theta\right)$$

$$\sigma_{22}(r,\theta) = \sigma_0\left(-\frac{a^2}{r^2}\left(\frac{1}{2}\cos 2\theta - \cos 4\theta\right) - \frac{3}{2}\frac{a^4}{r^4}\cos 4\theta\right)$$

$$\sigma_{12}(r,\theta) = \sigma_0\left(-\frac{a^2}{r^2}\left(\frac{1}{2}\sin 2\theta + \sin 4\theta\right) + \frac{3}{2}\frac{a^4}{r^4}\sin 4\theta\right)$$

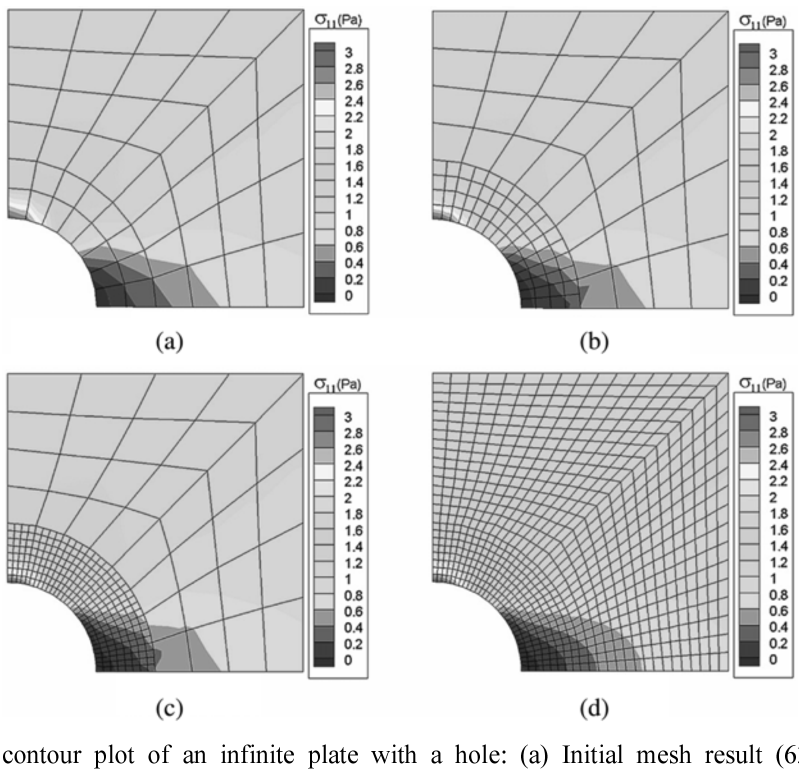

Fig. 10 The σ_{11} contour plot of an infinite plate with a hole: (a) Initial mesh result (63 nodes), (b) 1st adaptation result (121 nodes), (c) 2nd adaptation result (333 nodes), (d) 2nd reference result (825 nodes)

Table 2 Comparison of the maximum σ_{11} stress and relative error in energy norm between reference meshes and adaptation meshes

	Maximum σ_{11} stress at nearest Gauss point around 'A'	Relative error in energy norm at Ω_2
Coarse mesh (63 nodes)	2.663	0.152
Adaptation mesh 1 (121 nodes)	2.862	8.35×10^{-2}
Reference mesh 1 (221 nodes)	2.875	8.33×10^{-2}
Adaptation mesh 2 (333 nodes)	2.935	4.53×10^{-2}
Reference mesh 2 (825 nodes)	2.953	4.46×10^{-2}

The stress contour of σ_{11} are described in Fig. 10 and the numerical values of relative error norm and the maximum σ_{11} stress which is obtained at the nearest gauss point around 'A', are summarized in Table 2. Compared to the results of reference mesh, they show almost the same accuracy within 0.5% which seems to be affected by less number of degree of freedoms at the interface, not the limitation of proposed scheme.

5. Conclusions

In this paper, we present a new class of finite elements, based on the MLS method. In this class of elements, the space of the trial functions is significantly expanded compared with the conventional finite elements in that rational type shape functions are utilized for master elements. Moreover, they turn to polynomial type interpolation wherein Rank($\mathbf{W}$) is equal to NB by adjusting the domain of influence of individual nodes although they lead to rational type approximation in general. With this idea, $(4+n)$-noded finite elements which place an arbitrary number of nodes on edge are presented for connecting coarse mesh zone with fine mesh zone. To demonstrate the effectiveness and accuracy of the $(4+n)$-noded MLS-based elements, we have shown several numerical examples for capturing of high stress concentration using mesh gradation. They demonstrate that $(4+n)$-noded elements can be an effective tool to model complex structures consisting of two difference sizes of mesh by allowing proper mesh gradation. In addition to this, this element has a great potential in complex problems such as nonmatching contact problems, discontinuity propagations and so on.

Acknowledgements

This research was supported by a grant (06K1401-01010) from Center for Nanoscale Mechatronics & Manufacturing, one of the 21st Century Frontier Research Programs, which are supported by Ministry of Science and Technology, KOREA.

References

Aminpour, M.A., Ransom, J.B. and McCleary, S.L. (1995), "A coupled analysis method for structures with independently modeled finite element sub-domains", *Int. J. Numer. Meth. Eng.*, **38**, 3695-3718.

Aminpour, M.A., Krishnamurthy, T. and Fadale, T.D. (1998), "Coupling of independently modeled three-dimensional finite element meshes with arbitrary shape interface boundaries", AIAA paper, 98-2060.

Cho, Y.-S., Jun, S., Im, S. and Kim, H.-G. (2005), "An improved interface element with variable nodes for non-matching finite element meshes", *Comput. Meth. Appl. Mech. Eng.*, **194**, 3022-3046.

Cho, Y.-S. and Im, S. (2006), "MLS-based variable-node elements compatible with quadratic interpolation. Part I: Formulation and application for non-matching meshes", *Int. J. Numer. Meth. Eng.*, **65**, 494-516.

Cho, Y.-S. and Im, S. (2006), "MLS-based variable-node elements compatible with quadratic interpolation. Part II: application for finite crack element", *Int. J. Numer. Meth. Eng.*, **65**, 517-547.

Choi, C.K. and Lee, N.-H. (1996), "A 3-D adaptive mesh refinement using variable-node solid transition element", *Int. J. Numer. Meth. Eng.*, **39**, 1585-1606.

Choi, C.K. and Lee, N.-H. (1993), "Three dimensional transition solid elements for adaptive mesh gradation", *Struct. Eng. Mech.*, **1**, 61-74.

Choi, C.K. and Park, Y.M. (1989), "A nonconforming transition plate bending elements with variable mid-side nodes", *Comput. Struct*., **32**, 295-304.

Choi, C.K. and Park, Y.M. (1997), "Conforming and nonconforming transition plate bending elements for an adaptive h-refinement", *Thin-Walled Struct*., **28**, 1-20.

Farhat, C. and Roux, F.X. (1991), "A method of finite element tearing and interconnecting and its parallel solution algorithm", *Int. J. Numer. Meth. Eng.*, **32**, 1205-1227.

Gupta, A.K. (1978), "A finite element for transition from a fine to a coarse grid", *Int. J. Numer. Meth. Eng.*, **12**, 35-45.

Han, W. and Meng, X. (2001), "Error analysis of the reproducing kernel particle method", *Comput. Meth. Appl. Mech. Eng*., **190**, 6157-6181.

Hinton, E. and Campbell, J.S. (1974), "Local and global stress smoothing of discontinuous finite element functions using a least square method", *Int. J. Numer. Meth. Eng.*, **8**, 461-480.

Jin, X., Li, G. and Aluru, R.N. (2001), "On the equivalence between least square and kernel approximations in meshless methods", *Comput. Model. Eng. Sci*., **2**, 341-350.

Kim, H.-G. (2002), "Interface Element Method (IEM) for a partitioned system with non-matching interfaces", *Comput. Meth. Appl. Mech. Eng*., **191**, 3165-3194.

Lancaster, P. and Salkauskas, K. (1981), "Surface generated by moving least squares method", *Math. Comp.*, **37**, 141-158.

Lim, J.H., Im, S. and Cho, Y.-S., "MLS(Moving Least Square)-based finite elements for complex domains and discontinuities", *Int. J. Numer. Meth. Eng*., Accepted for Publication.

Lim, J.H., Im, S. and Cho, Y.-S., "MLS (Moving Least Square)-based finite elements for three-dimensional non-matching meshes and adaptive mesh refinement", *Comput. Meth. Appl. Mech. Eng*., Accepted for Publication.

Liu, G.R., Gu, Y.T. and Dai, K.Y. (2004), "Assessment and applications of point interpolation methods for computational mechanics", *Int. J. Numer. Meth. Eng*., **59**, 1373-1397.

Liu, W.K., Jun, S. and Zhang, Y.F. (1995), "Reproducing kernel particle methods", *Int. J. Numer. Meth. Fluids*, **20**, 1081-1106.

Pantano, A. and Averill, R.C. (2002), "A penalty-based finite element interface technology", *Comput. Struct*., **80**, 1725-1748.

Park, K.C., Felippa, C.A. and Rebel, G. (2002), "A simple algorithm for localized construction of non-matching structural interfaces", *Int. J. Numer. Meth. Eng*., **53**, 2117-2142.

Quiroz, L. and Beckers, P. (1995), "Non-conforming mesh gluing in the finite elements methods", *Int. J. Numer. Meth. Eng*., **38**, 2165-2184.

Timoshenko, S.P. and Goodier, J.N. (1970), *Theory of Elasticity(3rd edn)*. McGraw-Hill, New York.